Journal of Power Sources 190 (2009) 356–361

Contents lists available at ScienceDirect

Journal of Power Sources

journal homepage: www.elsevier.com/locate/jpowsour

Experimental and thermodynamic approach on proton exchange membrane fuel cell performance

Me. Miansari[a,*], K. Sedighi[b], M. Amidpour[c], E. Alizadeh[b], Mo. Miansari[b]

[a] Islamic Azad University Ghaemshahr, P.O. Box 163, Ghaemshahr, Iran
[b] Department of Mechanical Engineering, Noushirvani University of Technology, P.O. Box 484, Babol, Iran
[c] Department of Mechanical Engineering, K.N. Toosi University, Box 15875-4416, Tehran, Iran

ARTICLE INFO

Article history:
Received 18 May 2008
Received in revised form 21 December 2008
Accepted 18 January 2009
Available online 6 February 2009

Keywords:
PEM fuel cell
Exergy
Channel depth
Polarization curves
Irreversibilities
Experimental study

ABSTRACT

The present work is employed in two sections. Firstly the effect of different parameters such as pressure, temperature and anode and cathode channel depth on the performance of the proton exchange membrane (PEM) fuel cell was experimentally studied. The experimental result shows a good accuracy compared to other works.

Secondly a semi-empirical model of the PEM fuel cell has been developed. This model was used to study the effect of different operating conditions such as temperature, pressure and air stoichiometry on the exergy efficiencies and irreversibilities of the cell.

The results show that the predicted polarization curves are in good agreement with the experimental data and a high performance was observed at the channel depth of 1.5 mm for the anode and 1 mm for the cathode. Furthermore the results show that increase in the operating temperature and pressure can enhance the cell performance, exergy efficiencies and reduce irreversibilities of the cell.

1. Introduction

Increasing global energy consumption has had and will continue to have many detrimental effects on the earth's environment. One of the most noticeable results is the growing problem of air pollution around the earth [1]. On the other hand the depletion of fossil fuel and increase of oil price lead to new energy sources. The energy conversion technology which receives considerable attention recently is the fuel cell, a potential replacement for the conventional internal combustion engine.

The PEM fuel cell is an electrochemical energy conversion device, which converts the chemical energy of hydrogen and oxygen directly and efficiently into electrical energy, with waste heat and liquid water as by-products. A PEM fuel cell powered automobile using hydrogen, offers several advantages, such as low temperature operation and quick start-up that is compatible with renewable energy sources and can obtain a power density competitive with the internal combustion engine. However, the major barriers which are hindering the commercialization of PEM fuel cell powered automobiles are cost and hydrogen infrastructure.

One of the means of reducing the cost of PEM fuel cell powered automobile is by improving the performance of the PEM fuel cell itself. A proven method of enhancing the performance of energy and exergy analysis of the systems is optimization of operating conditions of the cell such as operating temperature, pressure and the gas channel depth. Djilali and co-workers [2,3] using a three-dimensional computational model for a single cell with an active area of 25 cm^2 and single-serpentine flow field, investigated the influence of this parameter on the cell performance. Recently Maher [4] has been investigating the effect of these parameters on cell performance by using the semi-empirical equations. Atul Kumar and Reddy [5] studied the effect of channel depth of the anode side on the hydrogen consumption using computational modeling.

Cownden et al. [6] performed the exergy analysis of the hydrogen fuel cell power system for bus transportation. Their work showed the usefulness of the thermodynamic analysis in determining the irreversibilities in different system components. Kazim [7,8] has conducted exergy analysis of a PEM fuel cell at specified operating voltages of 0.5 and 0.6 V. They reported the exergy efficiency of the PEM fuel cell at different operating conditions.

The present study experimentally investigated the effect of different parameters such as pressure, temperature and channel geometry at different operating voltages.

As experimental cost is too high a semi-empirical model was used to evaluate the polarization curve and finally exergy analysis was carried out to optimize the operating parameter for best performance of the cell.

* Corresponding author. Tel.: +98 9112154206; fax: +98 1113234205.
E-mail address: mmiansari@yahoo.com (Me. Miansari).

0378-7753/$ – see front matter © 2009 Elsevier B.V. All rights reserved.
doi:10.1016/j.jpowsour.2009.01.082

Nomenclature

A	cell area (cm^2)
C_p	specific heat ($kJ\,kg^{-1}\,K^{-1}$)
$C_{O_2}^{interface}$	oxygen concentration at the cathode membrane/gas interface ($mol\,cm^{-3}$)
ex	exergy ($kJ\,kg^{-1}$)
$F = 96{,}485$	Faraday constant ($C\,mol^{-1}$)
h	enthalpy ($kJ\,kg^{-1}$)
h_c	channel depth (mm)
I	current (A)
i	current density ($A\,m^{-2}$)
K	specific heat ratio
$\dot{m}$	mass flow rate ($kg\,s^{-1}$)
P	pressure (atm)
$P^*_{H_2}$	partial pressure of hydrogen at anode catalyst/gas interface (atm)
$\dot{Q}$	rate of heat lost (W)
r_M	membrane-specific resistivity for the flow of the hydrated protons ($W\,cm^2$)
S	entropy ($kJ\,kg^{-1}\,K^{-1}$)
T	temperature (K)
V	cell potential (V)
$\dot{W}$	power (W)
x	mole fraction

Greek letters

β	semi-empirical coefficients for calculation of activation overpotential
ε	cell efficiency (%)
η_{act}	activation overpotential (V)
η_{diff}	diffusion overpotential (V)
η_{ohmic}	ohmic overpotential (V)
λ	stoichiometry
μ	chemical potential ($J\,mol^{-1}$)

2. Fuel cell component

The PEM fuel cell system considered in the present study is a single cell with an active area of 25 cm^2 and single-serpentine flow field [9] geometries. The width and land width of the channel were selected to be 1 and 0.8 mm respectively.

The channel depth of 1 and 1.5 mm was considered for empirical work. For a bipolar plate, non-porous graphite [10] is selected.

A Nafion 117 membrane with 4 mg Pt cm^{-2} for the anode and cathode was employed as a membrane electrode assembly. On both sides of the MEA, there were 270-mm thick carbon papers that acted as diffusion layers. The experimental setup is shown in Fig. 1.

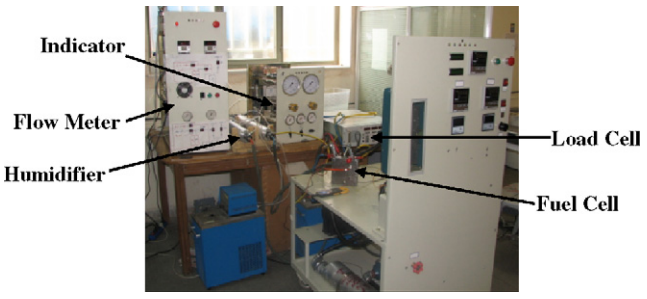

Fig. 1. Single cell with the experimental setup.

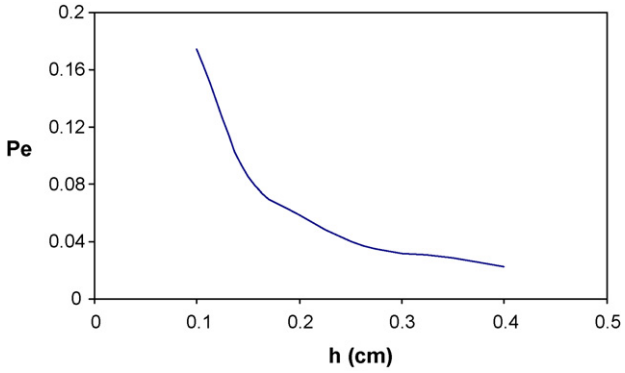

Fig. 2. Relative influence of convection (as determined by the Peclet number) for various channel depths.

3. Selection of channel dimension

3.1. Anode side

Kumar and Reddy [5] have simulated the performance of the anode side of the PEM fuel cell. Their work shows that for high hydrogen consumptions, the optimum dimensions for the channel width, land width and channel's depth were 1.5, 0.5 and 1.5 mm, respectively. But by considering the principle that an increase in the ribs' width causes diffusion mass limitation beneath the ribs and decreasing the sectional area of the channel can increase velocity of the gas in the channel and help in the removal of water droplet and lastly because of the construction problem and possibility of ribs breaking, the dimensions of the channel's width and land width were selected 1 and 0.8 mm respectively.

For the channel depth two dimensions of 1 and 1.5 mm for empirical work were considered.

3.2. Cathode side

Watkins et al. [11] studied the optimal dimensions for a bipolar channel on the cathode side of the fuel cell. They claimed the most preferred range to be 1.14–1.4 mm for the channel width, 0.89–1.4 mm for the rib width. So based on considering the principles which are presented in the anode side, the dimensions of 1 and 0.8 mm are used for channel width and rib width respectively.

For a selection of the channel depth at the cathode side, consider the two primary mechanisms for mass transport in fuel cells, binary diffusion and convection. In Refs. [12,13] these two mechanisms were considered and it was shown that if the convection dominates the transport, the cell would have a better performance.

One of the important criteria that influencing the convection is Peclet number, which compares the relative importance of the convection versus diffusion.

As it is distinguished in Refs. [12,14] the Peclet number depends on many parameters, so by holding porosity, permeability, channel length, channel and ribs width constant, the effect of the channel depth on the Peclet number was considered.

As is shown in Fig. 2, by increasing the channel depth, for the cathode side, more than 2 mm, the Peclet number will decrease and then the convection phenomenon and cell performance decrease especially in high current density.

So according to the result of this section and similar to the anode side, the two dimensions of 1 and 1.5 mm for the empirical work were considered.

As mentioned before in this section a semi-empirical model was employed to reduce the number of tests for evaluation of polarization curve.

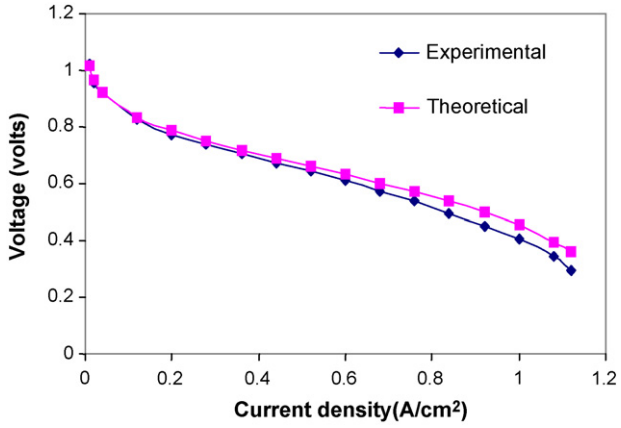

Fig. 3. Validation of analytical cell performance curve with experimental result.

4. Semi-empirical model of the fuel cell performance

Useful work is obtained from the fuel cell only when a current is drawn, but the actual cell potential (V) is decreased by its equilibrium thermodynamic potential (E_{Nernst}) because of irreversible losses. When the current flows, a deviation from the thermodynamic potential occurs corresponding to the electrical work performed by the cell. The deviation from the equilibrium value is called the overpotential (η).

Therefore, the expression of the voltage of a single cell is:

$$V = E_{\text{Nernst}} + \eta_{\text{act}} + \eta_{\text{ohmic}} + \eta_{\text{diff}} \tag{1}$$

When E_{Nernst} is the Nernst equation, η_{act} is the activation over voltage, η_{ohmic} is the ohmic over voltage, η_{diff} is the concentration over voltage. The terms of Eq. (1) are discussed in the following:

The Nernst equation for the reaction described above is [4]:

$$E_{\text{Nernst}} = 1.229 - 0.85 \times 10^{-3}(T - 298.15) + 4.3085 \times 10^{-5} T[\ln(P^*_{H_2}) + 0.5\ln(P^*_{O_2})] \tag{2}$$

where $P^*_{H_2}$, $P^*_{O_2}$ are the hydrogen and oxygen partial gas pressure (in atm) at the surface of the catalyst at the anode and cathode, respectively, and are shown as [15]:

$$P^*_{H_2} = (0.5P^{\text{sat}}_{H_2O})\left[\frac{1}{\exp(1.653i/T^{1.334}) \cdot x^{\text{sat}}_{H_2O}} - 1\right] \tag{3}$$

$$P^*_{O_2} = P[1 - x^{\text{sat}}_{H_2O} - x^{\text{channel}}_{\text{other gases}} e^{0.291i/T^{0.832}}] \tag{4}$$

where $x^{\text{sat}}_{H_2O}$ is the molar fraction of the water in a gas stream at saturation for a given temperature, $x^{\text{channel}}_{\text{other gases}}$ is the molar fraction of other gases (apart from oxygen) in the air steam. The molar fraction is:

$$x^{\text{sat}}_{H_2O} = \frac{P^{\text{sat}}_{H_2O}}{P} \tag{5}$$

The saturation pressure of water vapor can be computed from the following equation [2,16]:

$$\log_{10} P^{\text{Sat}}_{H_2O} = -2.1794 + 0.02253(T - 273.15) - (9.183 \times 10^{-5}) \times (T - 273.15)^2 (1.4454 \times 10^{-7})(T - 273.15)^3 \tag{6}$$

The molar fraction of other gases (mostly nitrogen) in the air stream is given by a log mean average between the molar fraction of nitrogen in a humidified stream of air at the inlet and the molar fraction at the outlet [15].

$$X^{\text{channed}}_{\text{other gases}} = \frac{X^{\text{in,hum}}_{\text{other gases}} - X^{\text{out,hum}}_{\text{other gases}}}{\ln[X^{\text{in,hum}}_{\text{other gases}} / X^{\text{out,hum}}_{\text{other gases}}]} \tag{7}$$

where

$$X^{\text{in,hum}}_{\text{other gases}} = 0.79(1 - x^{\text{sat}}_{H_2O}) \tag{8}$$

and

$$X^{\text{out,hum}}_{\text{other gases}} = \frac{1 - X^{\text{sat}}_{H_2O}}{1 + ((\lambda_{\text{air}} - 1)/\lambda_{\text{air}})(0.21/0.79)} \tag{9}$$

In Eqs. (8) and (9), the 0.79 term refers to the dry molar fraction of other gases in air, while in Eq. (9), the 0.21 term denotes the stoichiometry of the air stream.

4.1. Activation overpotential

The semi-empirical equation for the activation overpotential is [4]:

$$\eta_{\text{act}} = \beta_1 + \beta_2 T + \beta_3 T\ln(C^{\text{interface})}_{O_2}) + \beta_4 T\ln(I) \tag{10}$$

where

$$C^{\text{interface}}_{O_2} = \frac{P^*_{O_2}}{5.08 \times 10^6 \exp(-498/T)} \tag{11}$$

And the β coefficients are shown as:

$$\beta_3 = 0.000074, \quad \beta_4 = -0.000187, \quad \beta_1 = -0.9514, \quad \beta_2 = 0.00312$$

4.2. Ohmic overpotential

This could be expressed using Ohm's Law equations such as:

$$\eta_{\text{ohmic}} = -iR^{\text{internal}} \tag{12}$$

The total internal resistance is a complex function of temperature and current. A general expression for resistance is defined to include all the important membrane parameters:

$$R^{\text{internal}} = \frac{r_m L_m}{A} \tag{13}$$

The following empirical expression for Nafion membrane-specific resistivity is proposed [4]:

$$r_m = \frac{181.6[1 + 0.03(i) + 0.062(T/303)^2 i^{2.5}]}{[14 - 0.634 - 3i]\exp(4.18(T - 303/T))} \tag{14}$$

4.3. Diffusion overpotential

The total diffusion overpotential can be represented by the following expression [2]:

$$\eta_{\text{diff}} = m\exp(ni) \tag{15}$$

A physical interpretation for the parameters m and n were not given, but m correlates to the electrolyte conductivity and n to the porosity of the gas diffusion layer. The mass transfer coefficient m decreases linearly with the cell temperature but it has two different slopes as shown by the following expressions [2]:

$$m = 1.1 \times 10^{-4} - 1.2 \times 10^{-6}(T - 273.15) \quad \text{for } T \geq 312.15\,\text{K}(39^\circ\text{C}) \tag{16-a}$$

$$m = 3.3 \times 10^{-3} - 8.2 \times 10^{-5}(T - 273.15) \quad \text{for } T < 312.15\,\text{K}(39^\circ\text{C}) \tag{16-b}$$

5. Thermodynamic analysis

5.1. Exergetic analysis of a PEM fuel cell

The exergy method of analyzing energy systems integrates the first and second law of thermodynamics and reference environmental conditions. Exergy is defined as the maximum amount of work which can be obtained from a system or a flow of matter when it is brought reversibly to equilibrium with the reference environment. Every substance or system that is not in equilibrium with its reference environment has some quantity of exergy, while a substance or system in equilibrium with its reference environment has no exergy since it has no ability to cause any change with respect to its reference environment. The exergy consumption during a process is proportional to the entropy production due to irreversibilities. It is a useful tool for furthering the goal of more efficient energy use, as it enables the determination of the location, type and true magnitude of energy wastes and losses in a system.

The exergy of a stream of matter can be divided into different components. In the absence of nuclear, magnetism, electricity and surface tension effects, the specific total exergy is the sum of [17]:

$$ex = ex_{ke} + ex_{pe} + ex_{tm} + ex_{ch} \tag{17}$$

where ex_{ke}, ex_{pe}, ex_{tm} and ex_{ch} are the kinetic exergy, potential exergy, thermo mechanical exergy and chemical exergy, respectively. Since the changes in the kinetic and gravitational potential energies are considered to be negligible in the present study, physical exergy, which is the sum of kinetic, potential and thermo mechanical exergies, reduces to thermo mechanical exergy only.

The specific thermo mechanical exergy at a given state is defined as follows:

$$ex_{tm} = ex_{PH} = (h - h_o) - T_o(S - S_o) \tag{18}$$

The subscript 'o' represents the conditions of the reference environment that the temperature and pressure are $T_o = 298\,K$ and $P_o = 1$ atm respectively.

The physical exergy of an ideal gas with constant specific heat C_P and specific heat ratio K can be written as [7]:

$$ex_{PH} = C_P T_0 \left[\frac{T}{T_o} - 1 - \ln\left(\frac{T}{T_o}\right) + \ln\left(\frac{p}{p_o}\right)^{K-1/K} \right] \tag{19}$$

The chemical exergy is a result of the compositional imbalance between a substance and its reference environment. On a molar basis, the specific chemical exergy of a substance can be written as follows [18]:

$$ex_{ch} = \sum_j x_j(\mu_{jo} - \mu_{joo}) \tag{20}$$

where x_j is the mole fraction of the species j in the flow, μ_{jo} is the chemical potential of species j in the flow evaluated at T_o and P_o and μ_{joo} is the chemical potential of species j in the flow evaluated in the reference environment.

The equation for the rate of exergy destruction is [6]:

$$\dot{I}_{fc} = \left(1 - \frac{T_0}{T_{fc}}\right)\dot{Q}_{fc} - \dot{W} + \dot{m}_{H_2,R}(ex_{H_2})_R - \dot{m}_{H_2O,P}(ex_{H_2O})_P + \dot{m}_{air}(ex_{air,R} - ex_{air,P}) \tag{21}$$

where subscript R and P refer to exergies of the reactants and products, respectively.

The exergy efficiencies of the cell is defined as follows [7]:

$$\varepsilon = \frac{\dot{W}}{(\dot{E}_{air,R} + \dot{E}_{H_2,R})} \tag{22}$$

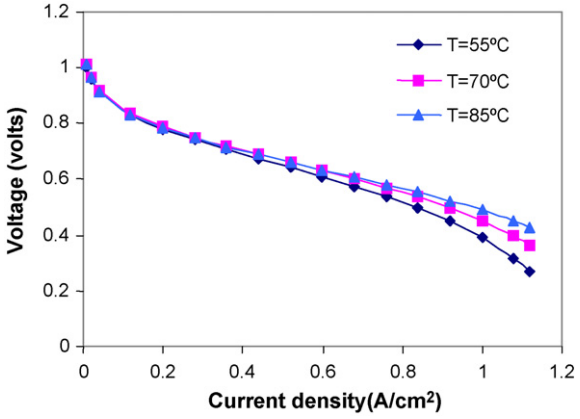

Fig. 4. Variation of cell performance at different operating temperature of cell.

It is notable that at standard atmospheric conditions, the air molar analysis (%) would be: $77.48N_2$, $0.03CO_2$, $20.59O_2$ and $1.9H_2O$.

The chemical exergy of the reactant air is taken to be zero, and it is assumed that the inlet flow is fully humidified and the mass flow rate of the water for humidification of the inlet flows are negligible.

The power produced by a single cell is given as:

$$\dot{W} = V \cdot I \tag{23}$$

6. Results and discussion

6.1. Experimental result

In Fig. 3, the analytical model was validated experimentally, so that the base-case operating conditions of the system temperature, pressure and air stoichiometric are 70 °C, 1 atm and 2 respectively.

The results show the predicted polarization curves are in good agreement with the experimental data. The slight difference between two curves can be due to variations in gases inlet, relative humidity and temperature between experimental and theoretical because of heat loses along the gas inlet pipes.

Figs. 4 and 5, show a series of polarization curves at different operating temperatures and pressures in the cell respectively. It can be seen that with the increase in temperature and pressure, the cell can operate with a higher performance. This is in fact due to the improvement in some parameters such as the exchange current density i_o of the oxygen reduction reaction, membrane conductivity κ, reversible thermodynamic potential E_{Nernst} and binary diffusivities D_{ij}.

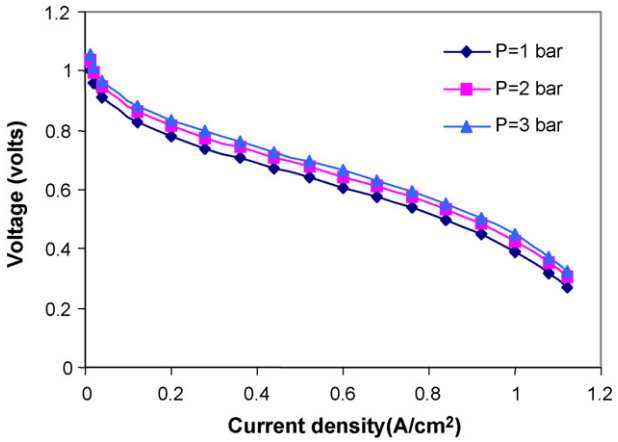

Fig. 5. Variation of cell performance at different operating pressure of cell.

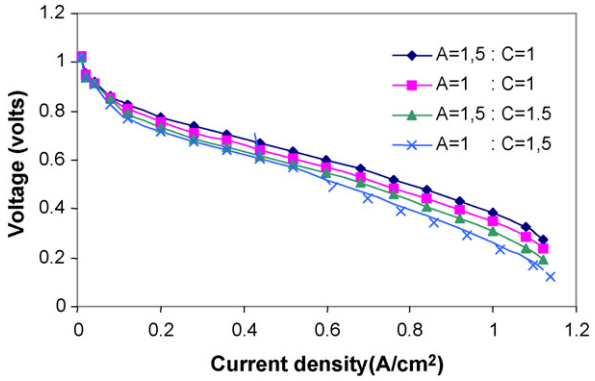

Fig. 6. The effect of channel depth on the cell performance.

Fig. 6 shows the effect of the channel depth at the anode and cathode side on the cell performance. As is clear in Fig. 6, the cell has higher performance at the channel depth 1.5 mm for the anode and 1 mm for the cathode.

Also according to Fig. 8 when the channel depth increases for the cathode and decreases for the anode, the cell performance shifts to a lower level. It can cause the decrease in velocity of the channel in the cathode side and therefore the Reynolds and Peclet number decrease and molecular diffusion outpaces transport by convection, also lack of sufficient water removal can be the cause for a lower performance.

AT anode side decrease in the channel's depth can cause the decrease in the hydrogen consumption.

6.2. Analytical result

The analysis presented above is integrated with the fuel cell performance model with the operating at varying temperatures, pressures and air stoichiometric ratios and current densities ranging from 0.01 to 1.12 A cm^{-2}. The base-case operating conditions of the system for temperature, pressure and air stoichiometric are, 70 °C, 1 atm and 2 respectively. The results are summarized in the plots shown in Figs. 7–11. Figs. 7 and 8 show the exergy efficiencies and irreversibilities of the cell at different operating pressure. The operating temperature was set as 70 °C, and the air stoichiometric was kept constant at 2. As shown in Fig. 7 the maximum exergy efficiencies are obtained as 52.8%, at a current density of 0.04 A cm^{-2} and the operating pressure of 3 atm and according to Fig. 8 irreversibilities of the cell decreased. These are due to decrease in irreversible losses, especially the anode and cathode overpotentials. With the increase in pressure, concentration of the reactants at the reaction sites increases, as a result the irreversible losses in the form of the anode and cathode overpotentials decreases, which in turn enhances the performance of the cell with the increase of the reversible thermodynamic potential according to the Nernst equation.

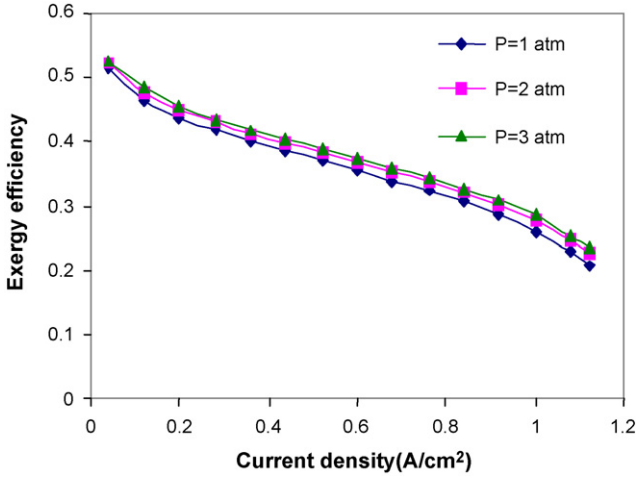

Fig. 7. Variation of exergy efficiency at different operating pressures of cell.

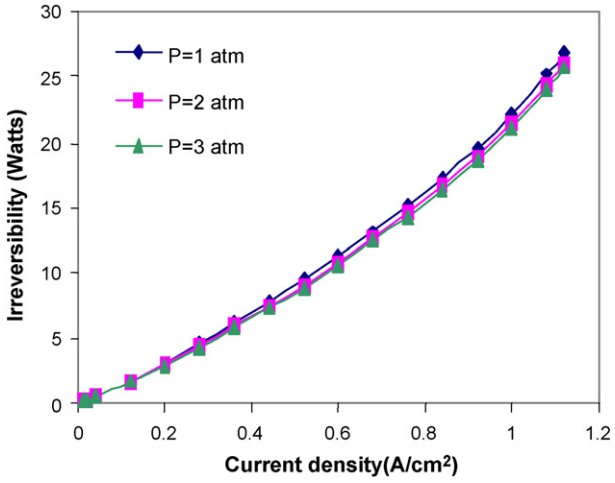

Fig. 8. Variation of irreversibilities at different operating pressures of cell.

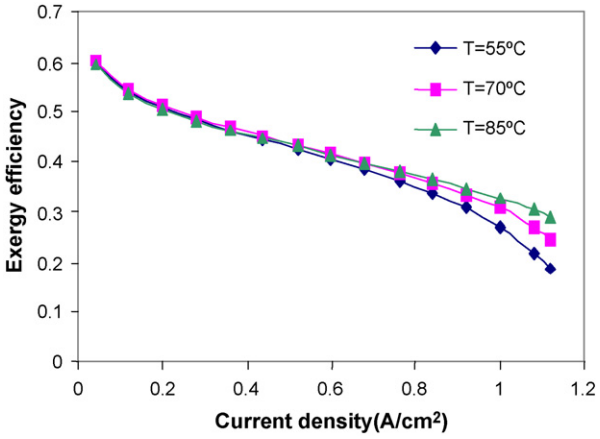

Fig. 9. Variation of exergy efficiency at different operating temperatures of cell.

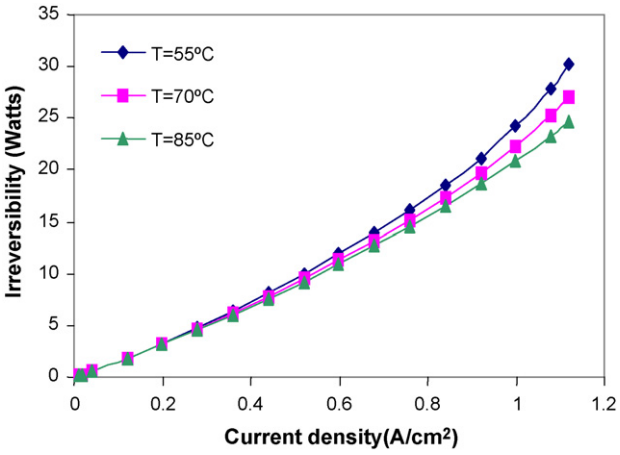

Fig. 10. Variation of irreversibilities at different operating temperatures of cell.

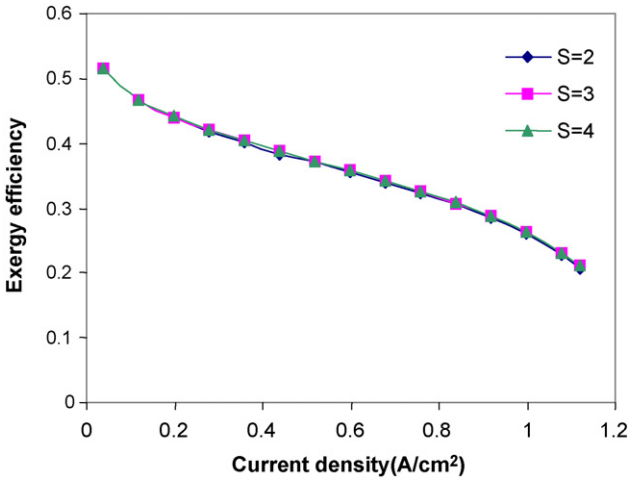

Fig. 11. Variation of exergy efficiency at different air stoichiometries of cell.

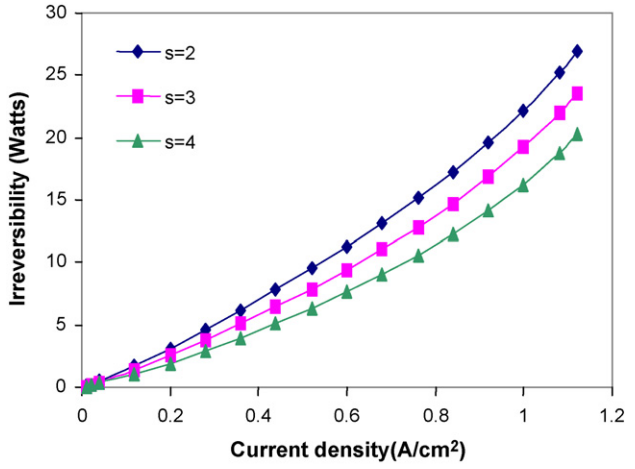

Fig. 12. Variation of irreversibilities at different air stoichiometries of cell.

Figs. 9 and 10 show the exergy efficiencies and irreversibilities of the cell at different operating temperatures of the cell. The operating pressure was set as 1 atm, and the air stoichiometric was kept constant at 2.0. It can be seen that with the increase of temperature, the exergy efficiencies of the cell increase and irreversibilities decrease. This is in fact due to the decrease in irreversible losses (irreversibility) of the cell with the increase of temperature, which in turn enhance the membrane conductivity and diffusion of proton in the membrane.

The variations of exergy efficiencies and irreversibilities of the cell at different air stoichiometries are shown in Figs. 11 and 12. The operating temperature and pressure were set as 70 °C and 1 atm. From the figures, it can be observed that irreversibilities decrease but there is no appreciable increase in exergy efficiencies with the increase in stoichiometry of air. With the increase of the air stoichiometry, molar flow rate of air increases resulting in the decrease of cathode overpotential.

7. Conclusions

An exergy analysis of a PEM fuel cell has been carried out. In addition, a parametric study is conducted to examine the effect of the varying operating conditions on the exergy efficiency of the cell. It was found that with the increase of cell operating temperature and pressure, exergy efficiency of the cell increases and irreversibilities decrease. No appreciable increase in exergy efficiencies was found with the increase of air stoichiometry.

Moreover, the experimental study of the effect of the operating conditions and gas channels depth on the cell performance, show that increase in the operating temperature and pressure can enhance the cell performance and also increase the channel's depth for the anode and decrease the channel's depth for the cathode side.

Thus, minimization of the irreversibility rate and enhancing the performance of the cell, can reduce the cost and help in commercialization of the fuel cell.

References

[1] I. Dincer, International Journal of Hydrogen Energy 27 (2002) 265–285.
[2] T. Berning, N. Djilali, Journal of Power Sources 124 (2005) 440–452.
[3] T. Berning, D.M. Lu, N. Djilali, Journal of Power Sources 106 (2002) 284–294.
[4] Maher A.R. Sadiq Al-Baghdadi, Renewable Energy 30 (2005) 1587–1599.
[5] A. Kumar, R.G. Reddy, Journal of Power Sources 113 (2003) 11–18.
[6] R. Cownden, M. Nahon, M.A. Rosen, International Journal of Exergy 1 (2) (2001) 112–121.
[7] A. Kazim, Energy Conversion and Management 45 (2004) 1949–1961.
[8] A. Kazim, Energy Conversion and Management 46 (2005) 1073–1081.
[9] X Li, I. Sabir, Journal of Hydrogen Energy 30 (2005) 359–371.
[10] A. Hermanna, T. Chaudhuri, P. Spagnol, Journal of Hydrogen Energy 30 (2005) 1297–1302.
[11] D.S. Watkins, K.W. Dircks, D.G. Epp, Novel fuel cell fluid flow field plate, US Patent 4,988,583 (1991).
[12] J.P. Feser, A.K. Prasad, S.G. Advani, Journal of Power Sources 161 (2006) 404–412.
[13] P.H. Oosthuizen, L. Sun, K.B. McAuley, Applied Thermal Engineering 25 (2005) 1083–1096.
[14] F. Barbir, H. Gorgun, X. Wang, Journal of Power Sources 141 (2006) 96–101.
[15] J. Wishart, M. Secanell, Z. Dong, Proceedings of the International Green Energy Conference, Waterloo, Ontario, Canada, June, 2005.
[16] S. Um, C.Y. Wang, K.S. Chen, Journal of the Electrochemical Society 147 (12) (2000) 4485–4493.
[17] Jan Szargut, David R. Morris, Frank R. Steward, Exergy analysis of thermal, chemical, and metallurgical processes, John Benjumins, New York, 1988.
[18] M.M. Hussain, J.J. Baschuk, X. Li, I. Dincer, International Journal of Thermal Sciences 44 (2005) 903–911.